Electrical Tuning of Optical Properties of Quantum Dot–Graphene Hybrid Devices: Interplay of Charge and Energy Transfer

Article *in* The Journal of Physical Chemistry C · April 2021

DOI: 10.1021/acs.jpcc.1c00643

CITATION
1

READS
43

5 authors, including:

Riya Dutta
Indian Institute of Science
6 PUBLICATIONS **22** CITATIONS
SEE PROFILE

Saloni Kakkar
Indian Institute of Science
12 PUBLICATIONS **66** CITATIONS
SEE PROFILE

Praloy Mondal
Indian Institute of Technology Bombay
23 PUBLICATIONS **442** CITATIONS
SEE PROFILE

Neha Chauhan
Indian Institute of Science
31 PUBLICATIONS **642** CITATIONS
SEE PROFILE

THE JOURNAL OF PHYSICAL CHEMISTRY C
A JOURNAL OF THE AMERICAN CHEMICAL SOCIETY

pubs.acs.org/JPCC

Article

Electrical Tuning of Optical Properties of Quantum Dot−Graphene Hybrid Devices: Interplay of Charge and Energy Transfer

Published as part of The Journal of Physical Chemistry virtual special issue "D. D. Sarma Festschrift".

Riya Dutta, Saloni Kakkar, Praloy Mondal, Neha Chauhan, and J. K. Basu*

Cite This: *J. Phys. Chem. C* 2021, 125, 8314−8322

Read Online

ABSTRACT: The combination of semiconductor quantum dots (QD) and single-layer graphene (SLG) can lead to the formation of optoelectronic devices with enhanced sensitivity and can have extensive applications in the field of the photodetector and photovoltaics. The optical properties of the resultant hybrid material are controlled by the interplay of energy transfer between QDs and charge transfer between the QDs and SLG. By studying the steady-state and time-resolved photoluminescence spectroscopy of hybrid QD−SLG devices, we observe a subtle interplay of short- and long-range energy transfer between cadmium selenide (CdSe) QDs in a compact monolayer solid film placed in close proximity to an SLG and the charge transfer from the QD solid to SLG. At larger separation, δ, between the compact monolayer QD and SLG, the emission properties are dominated by mutual energy transfer between the QDs. At relatively smaller separation the emission from QDs, which is strongly quenched, is dominated by charge transfer between QDs and SLG. In addition, we are also able to tune the relative strength of energy and charge transfer by electrostatic doping through the back gate voltage, which provides a novel pathway to tune emission properties of these devices for possible applications as photodetectors, in photovoltaics, and for sensing.

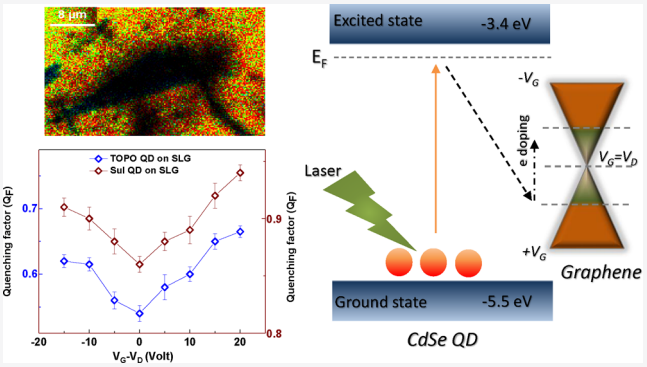

INTRODUCTION

Hybrid devices consisting of graphene and semiconductor quantum dots (QDs) have been widely studied for potential photodetector, photovoltaic,[1−3] and sensing applications.[4−6] While graphene possesses high electronic mobility, it has weak and wavelength-independent absorption.[7,8] In contrast, semiconductor colloidal QDs are strong light absorbers and emitters[9,10] with broad spectral tunability in the visible wavelength regime and beyond.[11,12] However, they have relatively poor carrier transport properties compared to graphene.[13,14] Consequently, combining these two classes of systems can lead to the formation of optoelectronic devices with enhanced sensitivity.[15−17]

While in some cases it is of interest to combine a single quantum emitter like QD with single-layer graphene (SLG),[8,18,19] it is beneficial in most applications, including photovoltaics or photodetector, to coat a film of QD on graphene.[20,21] Moreover, compact films of colloidal QDs are a new emergent class of materials called quantum dot solids with novel electrical[13,14] and optical properties.[22−25] An important aspect of these materials is the nature of energy or charge transfer between the individual QDs, which eventually determines their collective macroscopic electrical or optical properties. In particular, photoluminescence (PL) decay from these materials shows multiple components[26,27] corresponding to energy transfer between concentric shells of QDs. In this regard, we have also shown that emission from such compact monolayers of semiconductor QDs can be strongly quenched or enhanced[27−34] by suitably doping them with tiny metal nanoparticles (MNP) with the ability to generate localized plasmons upon irradiation with electromagnetic radiation. The emission properties depend, among other things, on the concentration of MNPs, their size, and the average separation between MNP-QD. We have recently shown that doping such materials with tiny plasmonic MNPs can lead to the emergence of quantum correlations and a novel strong coupling regime induced by many-body emitter-metal nanoparticle coupling at very small separations.[32]

At a fundamental level, the optoelectronic properties of QD−graphene based hybrid materials depend on the band

Received: January 24, 2021
Revised: March 23, 2021
Published: April 8, 2021

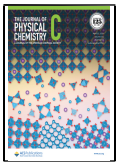

https://doi.org/10.1021/acs.jpcc.1c00643
J. Phys. Chem. C 2021, 125, 8314−8322

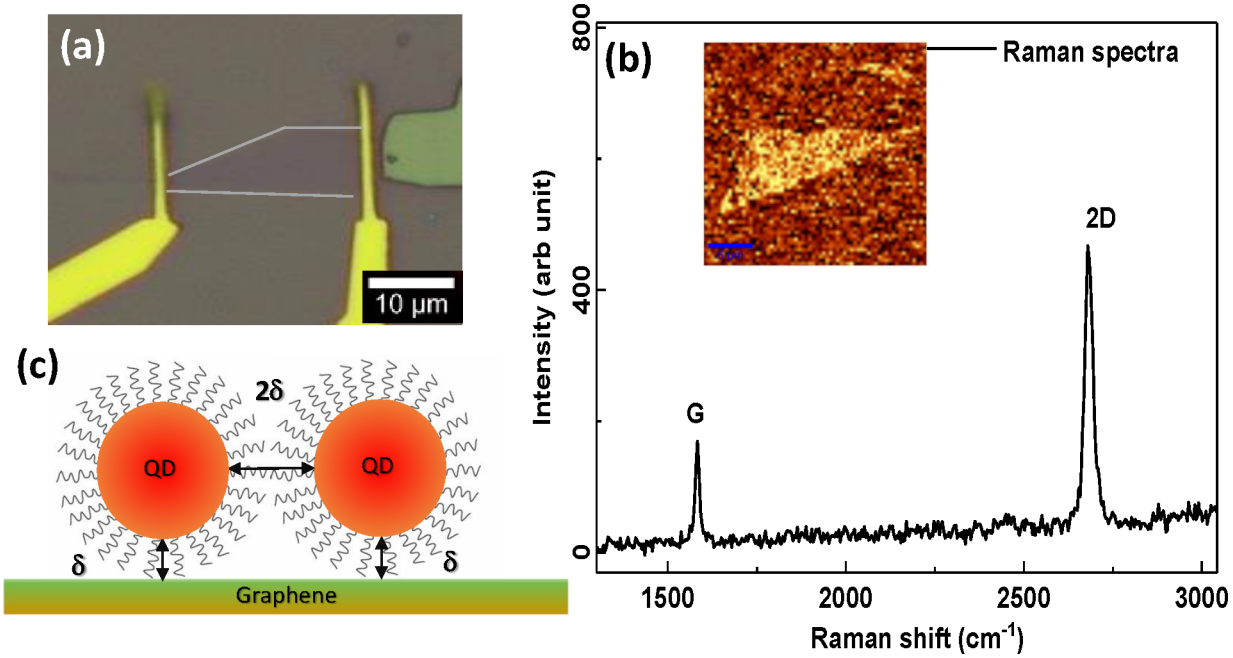

Figure 1. (a) Optical image of the single layer graphene FET device. The white line defines the edge of the graphene flake. (b) Characteristic Raman map and spectra from the graphene. (c) Surface separation between individual QDs and QD to graphene.

alignment of the QD used with respect to graphene.[35] While the QD band structure is fixed by it size and chemical properties,[36−38] graphene band structure is highly tunable through electrostatic gating or chemical doping, especially in a field-effect transistor device.[39−42] The optical properties of the resultant hybrid material are largely controlled by the extent of energy transfer between QDs[22,43] and charge transfer between the QDs and SLG.[35,44,45] While significant recent interest has been generated in understanding the novel emergent electrical[46,47] and optical properties[27−29,34,48] of compact colloidal QD films, there has been very little effort in exploring optoelectronic properties of compact QD film−graphene hybrid devices.[49] In particular, the interplay between the different energy and charge transfer channels has not been well studied.

Here we have used steady-state and time-resolved PL spectroscopy of hybrid QD−SLG FET devices to electrically tune the emission properties of quantum dots. We observe a subtle interplay of short- and long-range energy transfer between cadmium selenide (CdSe) QDs in a compact monolayer solid film placed in close proximity to a SLG and the charge transfer from the QD solid to SLG. At larger separation, δ, between the QD solid and SLG, the optical properties are dominated by mutual energy transfer between the QDs. However, at relatively shorter separation, engineered by changing the capping of the quantum dots, their emission, which is strongly quenched, is dominated by photoinduced charge transfer to the SLG. In addition, we can also tune the relative strength of energy and charge transfer by electrostatic doping, which provides a novel pathway to tune emission properties of these optoelectronic devices for possible applications as photodetectors, photovoltaics, and sensing.

EXPERIMENTAL SECTION

Materials. Cadmium oxide (CdO) powder, trioctylphosphine (TOP), trioctylphosphine oxide (TOPO), selenium powder, *n*-hexylphosphonic acid (HPA), potassium sulfide, formamide, acetonitrile, chloroform, and toluene were obtained from Sigma-Aldrich (Germany) for the synthesis of QDs and used as received.

Synthesis and Characterization of Quantum Dot. The CdSe quantum dots were prepared by the well-known hot-injection synthesis of CdSe cores, followed by a temperature-dependent growth. In a typical synthesis, CdO and trioctylphosphine oxide (TOPO) are mixed, and the mixture is heated up to 240 °C to get a clear solution, and then the solution heated up to 280 °C and inject the required amount of TOP-Se stock solution in the three-neck flux containing hot Cadmium based growth solution. A temperature of 280 °C for 4 min was used to get the proper size of QD. The QDs formed by the above-mentioned process showed PL emission maxima at 2.08 eV. The absorption and emission spectra are shown in Figure S1. The size distribution of the QDs have been estimated from TEM images (Figure S1b).

Device Fabrication and Characterization. Graphene FET has been made on highly doped silicon substrates with 285 nm silicon oxide layer. The substrates are cleaned in acetone and isopropyl alcohol to remove any residues and impurities. Graphene was exfoliated from graphite crystal by a well-known Scotch tape technique and placed onto the Si−SiO_2 substrate. The characteristics have been made by an optical microscope followed by Raman spectroscopy,[50,51] shown in Figure 1b, which suggests a single layer from the ratio of 2D to G peak emission intensities. The electron beam lithography technique is used for placing the gold contacts at the edge of the single-layer graphene. In this technique, we use the solution of the poly-methyl methacrylate (PMMA) layer to form a mask. The contacts are made by depositing 5 nm chromium/50 nm gold through the PMMA mask pattern in a thermal evaporation chamber under vacuum, and the contacts are bonded from the graphene device to the gold ports with gold wire.

To measure the graphene's transport characteristics in FET configuration, a small bias of 10 mV has been provided in the

https://doi.org/10.1021/acs.jpcc.1c00643
J. Phys. Chem. C 2021, 125, 8314−8322

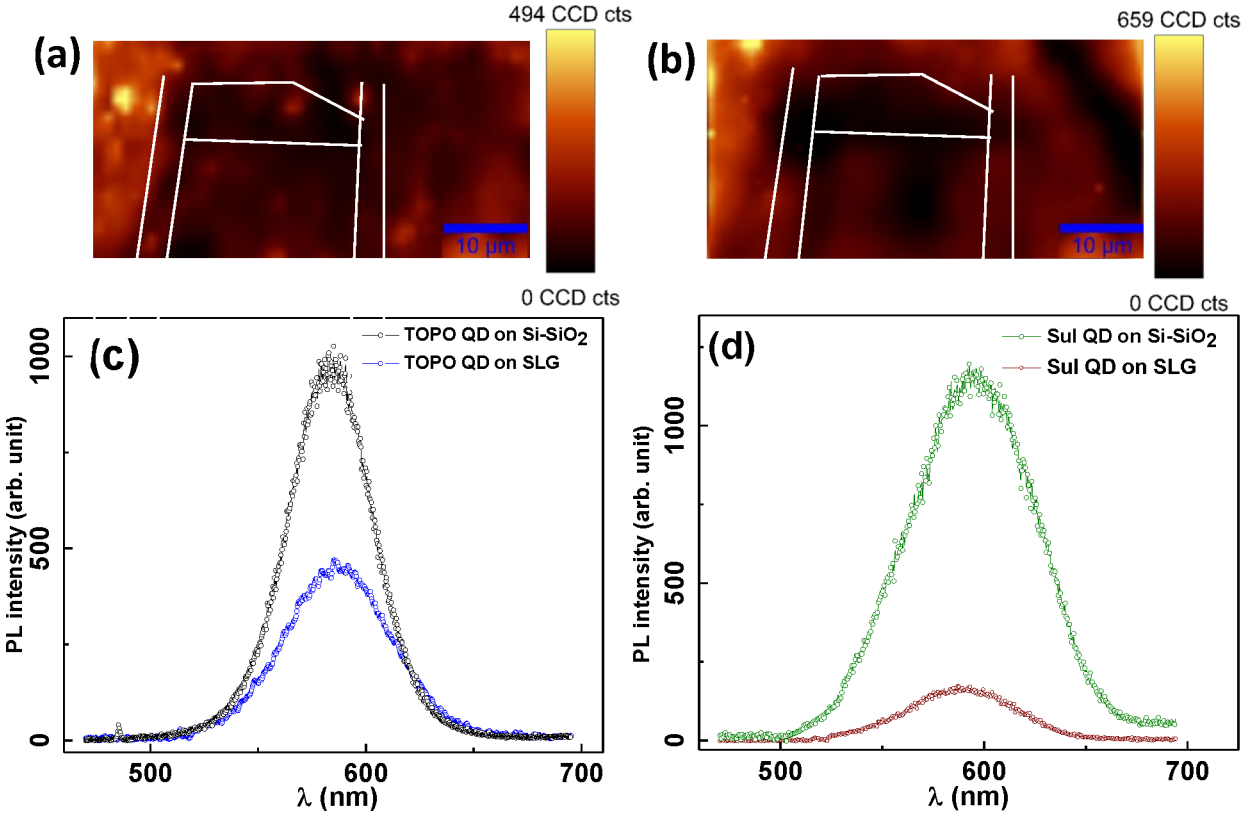

Figure 2. Steady state photoluminescence (PL) spectroscopy of hybrid devices. (a) PL intensity map shows the intensity variation of the TOPO QD layer on the graphene and on the Si−SiO_2 substrate. (b) PL intensity map for Sul QD on SLG FET system. (c) Corresponding PL spectra from reference TOPO QD on Si−SiO_2 substrate and on the SLG FET. (d) Similar PL spectra from reference Sul QD on Si−SiO_2 substrate and on the SLG FET.

channel, and by changing the doping through the gate, the current in the channel has been measured. The conductivity is a minimum near the Dirac point (V_D). Transport characteristics of graphene FET is plotted in Figure S2. The Dirac point of the pristine SLG FET device was measured to be 3.8 V.

Langmuir−Blodgett Technique for Monolayer Film Preparation. The Langmuir−Blodgett (LB) technique has a broad impact on single-layer formation since it has meticulous control over the internal structure up to the molecular level. Here QDs are mixed with volatile solvent chloroform and spread over deionized water (18.2 MΩ, Millipore) filled Langmuir trough (Kibron MicroTrough G-series, Finland). The QDs are compressed by a hydrophobic Teflon barriers from both side of the trough and with sufficient compression leading to the formation of a compact monolayer. The graphene FET device picks up the monolayer of QDs from the top of the trough surface. The layer has been transferred at surface pressure of 38 mN/m. The compression isotherm has been shown in Figure S3 (Supporting Information). The formation of compact layer and height difference has been confirmed by AFM topography map. The AFM map and corresponding height profiles are provided in Figure S4 (Supporting Information).

Ligand Exchange Procedure. For the ligand replacement, we have followed a well-known ligand exchange procedure.[52−56] The ligands can be replaced by different procedures in the solution, film, and vapor phase. Here, we have replaced the long-chain ligand TOPO with shorter chain length of sulfur by vapor phase method. For the replacement procedure, we have used a solution of potassium sulfide (K2S) and formamide. The vapor of the particular solution has been exposed to the films under a nitrogen gas environment for 10 h and furthermore followed by a vapor expose with toluene solvent to remove excess previous capping TOPO. For the confirmation of ligand replacement, we have performed atomic force microscopy (AFM) imaging before and after the ligand exchange procedure (Supporting Information Figure S4).

Steady State and Time Resolved PL Spectroscopy. The steady-state PL spectroscopy measurements have been performed in confocal mode (WiTec alpha-300 SNOM setup). The sample is excited with a 100× air objective, and the emission signal is collected in reflection geometry. We have used a notch filter and a long pass dichroic beam splitter to separate out the laser line. The emission signals are collected by a charge-coupled device detector. We have also studied the exciton decay behavior of respective systems. TRPL measurement has been performed with MicroTime 200 (Picoquant, Germany) fluorescence lifetime microscope. The sample is excited with a fiber-coupled pulsed laser diode of laser source of 507 nm. The repetition rate has been selected at 10 MHz to ensure maximum lifetime range. We have used a 100× air objective that is used to excite and collect signals from the samples. Measurement and analysis have been performed using the software SymPhoTime 64 (Picoquant, Germany). All measurements were performed at constant incident power of 20 μW in ambient conditions.

■ RESULTS AND DISCUSSION

In this study, we have used two specific configurations of QD coated single-layer graphene (SLG) field-effect transistor

https://doi.org/10.1021/acs.jpcc.1c00643
J. Phys. Chem. C 2021, 125, 8314−8322

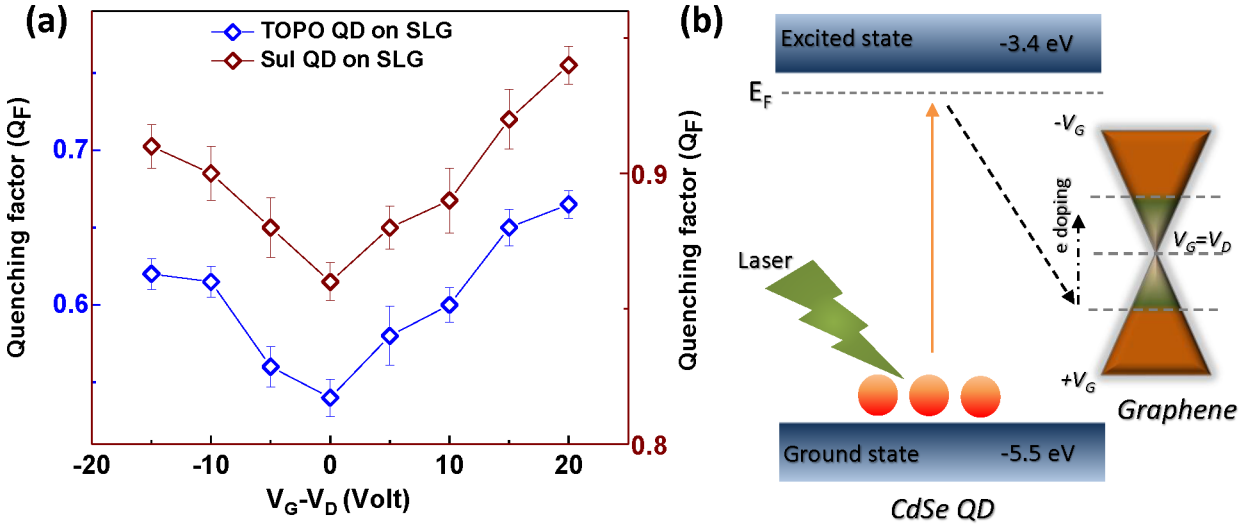

Figure 3. (a) Quenching factor (Q_F) of the QD PL emission in the presence of graphene with respect to the reference QD system. The quenching is more in the case of SuI QD on SLG FET system (right panel). (b) QD−graphene composite system's band alignment diagram.

(FET). In the first case. A single layer of TOPO capped QDs have been transferred on SLG FET. The surface separation is dictated by the dielectric ligands attached to the surface of QDs. Now we have another similar geometry where the QDs are placed closely with lesser surface separation emerging due to shorter dielectric ligand of sulfur (SuI). In the first case of TOPO QD on SLG, the surface−surface separation between QDs, $2 \times \delta$, is ∼2.2 nm,[32,57,58] while for SuI QD this value is reduced to ∼0.6 nm (Figure 1c).[59] The corresponding separations, δ, between the QDs and graphene are 1.1 and 0.3 nm, respectively, for TOPO and SuI QD on SLG. Figure 1a shows the optical image of the single-layer graphene in FET configuration. The existence of a single layer has been confirmed by Raman characterization (Figure 1b). The main first-order Raman band in graphene, known as the G band (1580 cm^{-1}), is a doubly degenerate in-plane sp^2 C−C stretching mode. The most substantial peak in graphene is the 2D band (2700 cm^{-1}), a second-order Raman process.

Figure 2a shows the PL intensity map for TOPO QDs on the graphene FET device for a particular gate voltage, $V_G = V_D$. A similar map is shown in Figure 2b for the SuI QD system. The maps represent the spatial variation of steady-state PL intensity of respective QDs on SLG and outside the SLG flake. Strong quenching of QD's PL intensity is observed on the graphene flake, while regions outside the graphene show brighter intensity. To quantify the PL intensity variation between QDs on Si−SiO_2 and on SLG, we compare the steady-state PL spectra from several regions on Si−SiO_2 and SLG. Figure 2c shows one such individual PL spectrum for TOPO QD on Si−SiO_2 and SLG, while Figure 2d shows the same for SuI QD system for $V_G = V_D$. Quenching of PL on SLG compared to that on Si−SiO_2 is clearly observed in these spectra similar to earlier observations of QDs on graphene.[19−21] Experimentally, PL quenching factor (Q_F) is defined as

$$Q_F = \left[1 - \frac{I_{QD-SLG}}{I_{ref.QD}}\right] \times 100\% \quad (1)$$

where, I_{QD-SLG} and $I_{ref.QD}$ are defined as the PL intensity from QD on SLG and reference QD on Si−SiO_2, respectively. Here, we have considered single point PL spectra from multiple regions of QD layer on SiO_2 and on SLG. The Q_F is calculated as the ratio of the mean of the maximum intensity of these several spectra (15−20 spectra) from the QD on SLG to that of ref QD. From the PL spectra in Figure 2c we estimated Q_F to be ∼54% for TOPO CdSe QDs placed on SLG. This factor further increases to 86% for the SuI QD on SLG when δ reduces to 0.3 nm.

We now explore the possible variation of Q_F with V_G. In Figure 3a, we show V_G dependence of Q_F. The quenching factor is observed to be a minimum near the Dirac point, V_D. What is also clear is the significant enhancement of this quenching factor with a reduction in d in the SuI based FET device. Nonradiative energy transfer between QDs and graphene can occur by resonant energy transfer (RET) or by charge transfer (CT).[19] Both these processes have a well-known dependence on δ.[8,18,60−63] In addition there is a possibility of RET between QDs which also has a well-known dependence on $2 \times \delta$.[19] The extent of PL quenching will be decided by the interplay of these competing processes. CT or RET depends on the band alignment between QDs and graphene as explained in Figure 3b. Since the Fermi energy of graphene can be tuned by varying V_G, this suggests electrical control of CT or RET between QD monolayer and graphene and hence the emission of the QD monolayer. However, to obtain insight into which out of the two possible processes dominate the PL of the QDs, steady-state PL alone is insufficient, and hence we now consider time-resolved PL measurements on these FET devices as well. The temporal dependence of the PL intensity is defined by

$$I(t) = Ae^{-\kappa t} \quad (2)$$

where κ is the decay rate. In the case of compact quasi-ordered QD films, the TRPL data are often found to be best described by a multiexponential function indicative of nearest and next nearest neighbor energy transfer between QDs.[27,28,30,32] The decay profiles were thus fitted with triple exponential decay functions of the form

$$I(t) = A_1e^{-t/\tau_1} + A_2e^{-t/\tau_2} + A_3e^{-t/\tau_3} \quad (3)$$

and

https://doi.org/10.1021/acs.jpcc.1c00643
J. Phys. Chem. C 2021, 125, 8314−8322

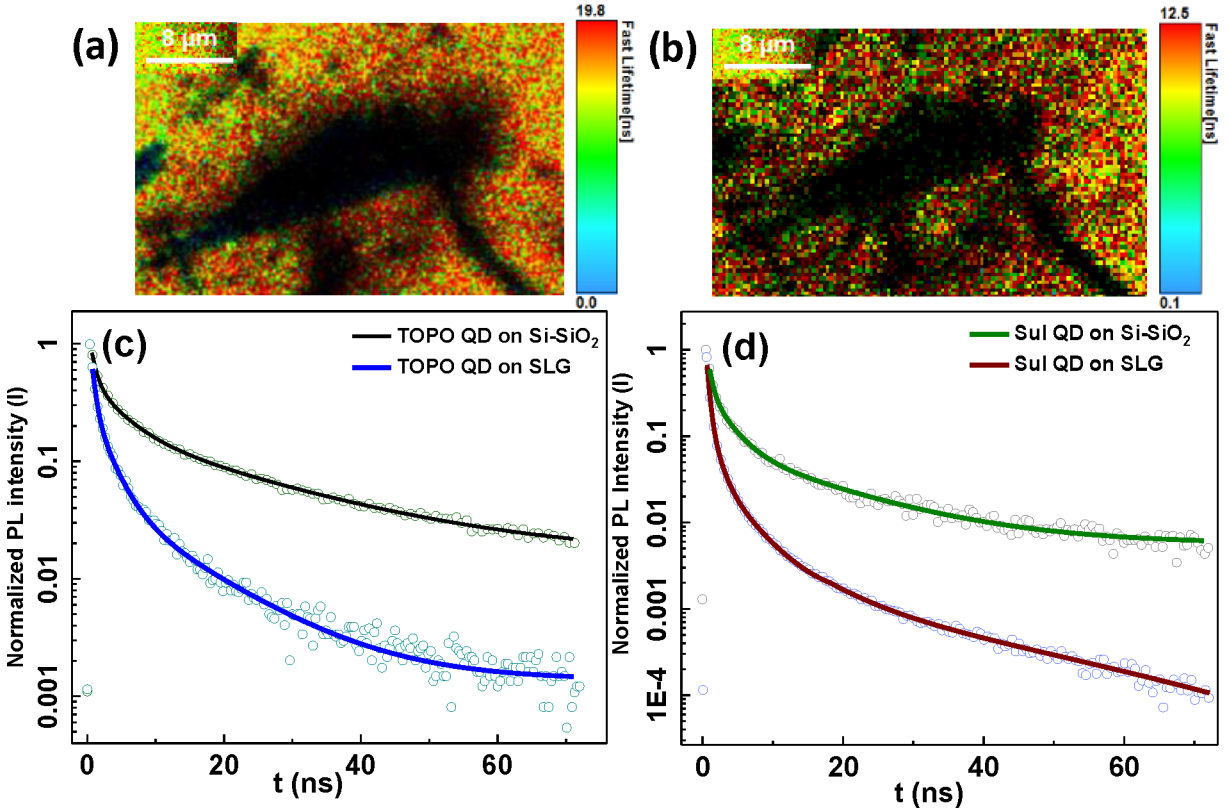

Figure 4. Time resolved photoluminescence (TRPL) study of different systems, showing the intensity variation topography map of (a) TOPO QD on SLG FET and (b) SuI QD on SLG FET from the TRPL measurement. (c) Decay spectra from reference TOPO QD on Si−SiO_2 substrate and on the SLG FET. (d) The same decay spectra from reference SuI QD on Si−SiO_2 substrate and on the SLG FET.

Table 1. Fitted Parameters ($V_G = V_D$)[a]

sample	τ_1 (ns) (A_1)	τ_2 (ns) (A_2)	τ_3 (ns) (A_3)	τ_{avg} (ns)
T QD−SiO_2E	0.82 ± 0.04 (34 ± 0.16%)	4.6 ± 0.3 (39 ± 0.14%)	19.7 ± 1 (27 ± 0.13%)	15.3 ± 0.4
T QD−SLG	0.53 ± 0.03 (62.7 ± 0.9%)	2.4 ± 0.2 (31.1 ± 0.2%)	12.6 ± 0.6 (6.2 ± 0.12%)	6.4 ± 0.2
S QD−SiO_2	0.56 ± 0.04 (56.7 ± 0.11%)	2.9 ± 0.2 (32.7 ± 0.2%)	16.7 ± 1 (10.6 ± 0.14%)	10.7 ± 0.3
S QD−SLG	0.49 ± 0.02 (92.6 ± 0.8%)	2.1 ± 0.1 (6.5 ± 0.3%)	10.15 ± 0.4 (0.9 ± 0.02%)	2 ± 0.1

[a]The table shows calculated parameters from TRPL measurement by fitting a particular set of spectra. The errors esimated from multiple meausrement have been provided in Figure 5S and in Figure S5. Here T QD represnets TOPO QD and S QD represents SuI QD.

$$\tau_{avg} = \frac{\sum A_i \tau_i^2}{\sum A_i \tau_i} \quad (4)$$

Here, τ_i's are the different decay lifetime component and A_i represents the corresponding probability amplitudes. Further, the corresponding decay rate components can be written as

$$\kappa_i = \frac{1}{\tau_i} \quad (5)$$

Three exponential decays are typical in such compact QD layers and have been reported by us[27] and others[26,64] earlier. The different rates correspond to energy transfer between a particular QD and various concentric shells of QDs surrounding this QD. Figure 4a represents the lifetime and PL intensity map for the TOPO QD based graphene FET devices, while Figure 4b represents the same for the SuI QD based FET device. Similar to the steady-state PL map, we observe quenching of lifetime of QDs on graphene compared to that on surrounding Si−SiO_2. To quantify the time-dependent PL, we compare typical data for QDs on Si−SiO_2 and SLG in Figure 4c for TOPO QDs. A clear reduction of the lifetime can be observed. Similar behavior with even stronger quenching is observed for SuI QD FET in Figure 4d. By fitting all TRPL data to eq 3, we obtain information about the various lifetime components of QDs, their modifications due to energy transfer, and the dependence on δ. Table 1 shows one such set of comparative fitted parameters for $V_G = V_D$.

We are now in a position to explore the interplay of RET between QDs and either CT or RET between QD and SLG and also demonstrate how this can also be tuned by electrostatic doping of the FET devices. Several key observations can be noted from the data presented in Table 1. For TOPO QDs on Si−SiO_2 τ_1 and τ_2 have almost equal weighting, although their actual values are significantly different. The longest component τ_3 is smaller than these two components but otherwise still significant. As shown earlier,[27,32,64] the shortest lifetime component, τ_1, corresponds to that originating from nearest neighbor RET interactions between QDs. A strong reduction of an average lifetime τ_{avg} of TOPO capped QD from 15.3 to 6.4 ns by introducing this QD layer on SLG is observed. While the contribution of τ_1 increased to 63%, that of τ_3 decreased to 6.2% . Both τ_1 and

https://doi.org/10.1021/acs.jpcc.1c00643
J. Phys. Chem. C 2021, 125, 8314−8322

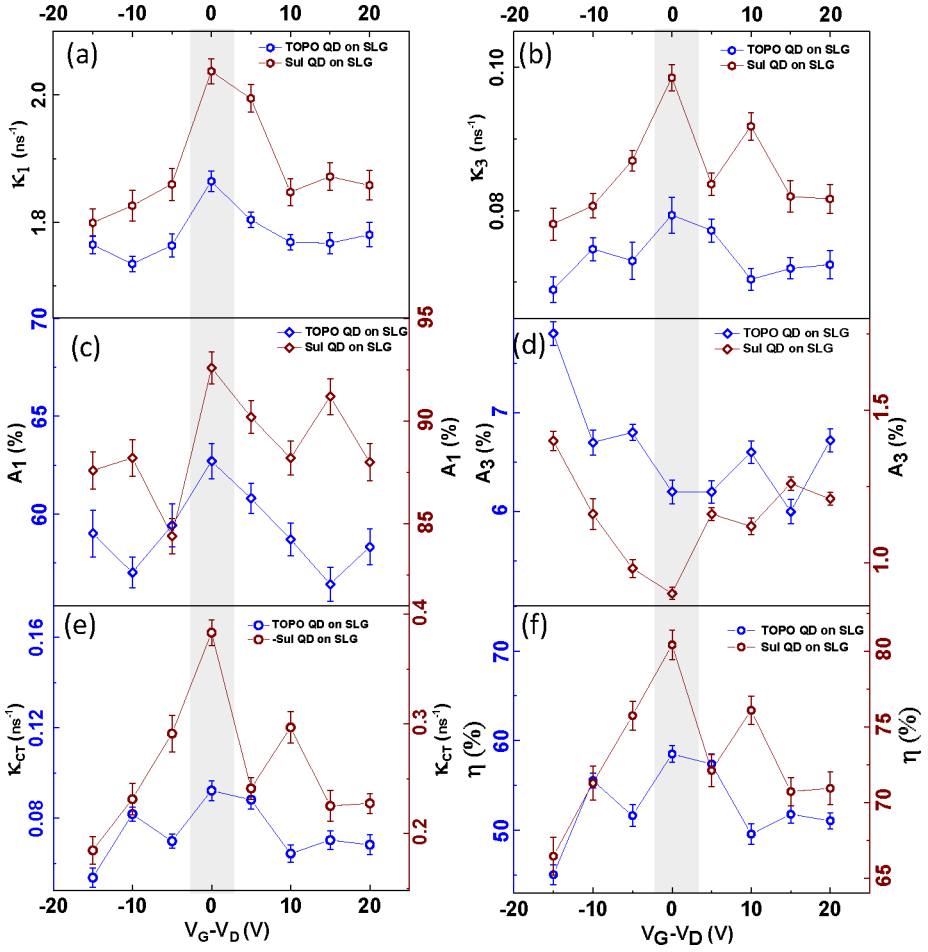

Figure 5. Decay rate components of QDs on graphene. (a) Decay rate (κ_1) corresponding to shortest component (τ_1) and (b) κ_3 to the longest component (τ_3) for the system of TOPO QD on SLG and Sul QD on SLG. Corresponding contribution of the decay rates (c) A_1 and (d) A_3. (e) Charge transfer rate (κ_{CT}) and (e) charge transfer efficiency (η) as a function of external doping.

τ_3 decreased. It occurs because of the additional energy transfer channel which is available on graphene. For Sul QD FET devices, we observe that even on Si−SiO_2, there is a reduction of all lifetime components compared to that with TOPO. This is driven purely by RET between QDs, which significantly increases due to a reduction in $2 \times \delta$. However, in this case, the τ_1 component becomes dominant while τ_3 becomes comparatively smaller. On SLG for the same system, we observe a dramatic enhancement of the relative contribution of τ_1 component. In contrast, that of τ_3 becomes almost insignificant, suggesting the dominance of QD−SLG energy transfer for these systems. As a result, there is a sharp decrease in τ_{avg} by more than a factor of 5. We now try to understand what is the dominant mechanism of decay rate modification of QDs by graphene: RET or CT. If we consider the additional contribution[65,66] to the decay rate due to graphene as κ_G and the following relation to be valid,

$$\kappa_{QD-SLG} = \kappa_{ref.QD} + \kappa_G \tag{6}$$

where $\kappa_{ref.QD}$ and κ_{QD-SLG} are the decay rate of reference QD systems and the same QDs in the presence of graphene. Then any possible RET based energy transfer between QDs and graphene can be considered. This aspect has been well studied for the QD−graphene system, including its δ dependence, so it should be possible to check this easily. Using the data in Table 1 and the above eq 6, we find κ_G to be 9.2×10^{-2} ns^{-1} for TOPO QD on SLG device while it is 38.3×10^{-2} ns^{-1} for the Sul QD on SLG device. In addition we can also calculate the decay rate efficiency, η, from the corresponding rate as[65]

$$\eta = 1 - \frac{\kappa_{ref.QD}}{\kappa_{QD-SLG}} \tag{7}$$

Using eq 7, we evaluate a decay rate efficiency, η, to be 58.5% for TOPO QD with a δ value of 1.1 nm and a significantly enhanced value of 81% for the Sul QD system with δ of 0.3 nm.

However, if we now cross-check the dependence of κ_G on δ, we obtain a ratio of 4.16. We now explore the possibility of CT for these QD based systems. In order to estimate the δ dependence, we use the well-known Marcus model[66,67] for CT wherein κ_{CT} is defined as

$$\kappa_{CT} = CV^2 \tag{8}$$

where V denotes the electronic coupling strength. According to previous reports,[66,68,69] the strength (V) reduces exponentially with distance, and it can be expressed in terms of an exponential distance-dependent decay function as[66,68,69]

$$V = V_0 \exp(-\delta) \tag{9}$$

where V_0 is constant termed as the rate at close contact[69] and δ is the surface separation. By considering the known values of δ for TOPO QD on SLG[32,57,58] and for Sul QD on SLG,[59] we

https://doi.org/10.1021/acs.jpcc.1c00643
J. Phys. Chem. C 2021, 125, 8314−8322

obtain an expected δ dependence of 4.95 from eq 8, using eq 9, while from our calculated ratio of κ_G we obtain a value of 4.16. Since it is clear that charge transfer is the dominant process of interaction between the QDs and SLG, especially when the separation δ is low, the additional contribution to the decay rate due to graphene, κ_G as indicated in eq 6, can be identified as the charge transfer rate κ_{CT}.

Further insight can be obtained by also exploring the V_G dependence of the decay rates. In Figure 5a,b, we present V_G dependence of κ_1 and κ_3, respectively, for Sul QD on SLG as compared to TOPO QD on SLG. We observe decay rate enhancement when δ reduces in the Sul QD-based system compared to TOPO QD based system. However, doping of the FET significantly alters this enhancement, which is maximum at the Dirac point. Thus, CT effects start decreasing away from the charge neutrality point of the device. In terms of the probability of the various decay channels, we observe in Figure 5c,d that while the κ_1 channel probability, represented by A_1, is maximum at $V_G = V_D$, that of the κ_3 channel (A_3) shows opposite trends being minimum at the same V_G. As explained earlier and discussed by us[27,29] and others,[26] κ_3 corresponds to long-range energy transfer between QDs in compact films. By tuning the Fermi energy E_F of the SLG channel through V_G, it is possible to reduce the probability of CT. Suppression of CT leads to enhancement of the possibility of long-range RET between QDs. Finally, in Figure 5e,f we demonstrate V_G dependence of κ_{CT} and η. We observe maximum CT probability near the Dirac point, which is consistent with the conclusions from Figure 5a−d as well as from Figure 3. While the reduction in δ affects both κ_1 and κ_3, the effects are stronger for the former decay rate. In a reference system consisting of only the QD solid monolayer films on Si−SiO_2 where no charge transfer takes place, while we do observe decay rate enhancement due to reduction in 2δ (Figure S5), the extent of enhancement is significantly smaller and, expectedly, independent of V_G. We would also like to note here the significant difference in the energy transfer process between QDs in the presence of MNPs, as shown earlier,[27,32,64] and that in the presence of graphene. In QD compact monolayers doped with MNPs decay rates are observed to change due to RET between QDs and MNPs as compared to the pure QD monolayers without altering the relative weight of the various components. For the QD−SLG system we observe drastic increase of the weight factor corresponding to nearest neighbor QD interaction decay rate (τ_1) at the expense of the rest and especially the long-range component (τ_3). Thus, our study not only highlights the interplay between charge and energy transfer through electrical control but also highlights important differences with the dominant energy transfer processes in quantum dot solid due to presence of tiny metal nanoparticles where charge transfer is negligible and either quenching or PL enhancements can be observed.

CONCLUSIONS

Using steady-state and time-resolved photoluminescence measurements on core CdSe quantum dot−graphene hybrid optoelectronic devices, we report a change in emission properties of the compact quantum dot monolayer solids by altering the extent of dot−dot energy or dot−graphene charge transfer. The interplay between charge and energy transfer was tuned by varying both the dot−dot and dot−graphene distance as well as the Fermi energy of graphene by varying the back gate voltage in the FET devices. We also reveal how graphene mediated charge transfer alters the energy transfer probability between quantum dots in nearest and next nearest neighbor multilayer shells. We also indicate how this differs from interaction between metal nanoparticles and QDs in similar quantum dot solids where nonradiative energy transfer mediated quenching or superradiance has been observed. Our demonstrated electrical control of optical properties of compact quantum dot solids mediated by their interactions with proximal graphene layer can lead to possible applications of these hybrid optoelectronic materials in photovoltaics and photodetector devices.

ASSOCIATED CONTENT

Supporting Information

The Supporting Information is available free of charge at https://pubs.acs.org/doi/10.1021/acs.jpcc.1c00643.

Characteristic measurements of quantum dots that include UV−vis spectroscopy, TEM images, Raman spectroscopy of single layer graphene, transport characteristics, Langmuir−Blodgett compression isotherm, AFM image of compact layer, and time-resolved PL decay spectra (PDF)

AUTHOR INFORMATION

Corresponding Author

J. K. Basu − *Department of Physics, Indian Institute of Science, Bangalore 560012, India*; orcid.org/0000-0002-6683-4732; Email: basu@iisc.ac.in

Authors

Riya Dutta − *Department of Physics, Indian Institute of Science, Bangalore 560012, India*

Saloni Kakkar − *Department of Physics, Indian Institute of Science, Bangalore 560012, India*

Praloy Mondal − *Department of Physics, Indian Institute of Science, Bangalore 560012, India*

Neha Chauhan − *Department of Physics, Indian Institute of Science, Bangalore 560012, India*

Complete contact information is available at: https://pubs.acs.org/10.1021/acs.jpcc.1c00643

Notes

The authors declare no competing financial interest.

ACKNOWLEDGMENTS

We acknowledge the Department of Science and Technology and Science and Engineering Research Board (SERB), India, for the financial support and the Advanced Facility for Microscopy and Microanalysis (AFMM), Indian Institute of Science, Bangalore, for the access to TEM measurements. R.D. acknowledges DST, Inspire, for financial support. We acknowledge Prof. Arindam Ghosh for the helpful discussions.

REFERENCES

(1) Kovalenko, M. V. Opportunities and challenges for quantum dot photovoltaics. *Nat. Nanotechnol.* **2015**, *10*, 994−997.

(2) Nurmikko, A. What future for quantum dot-based light emitters? *Nat. Nanotechnol.* **2015**, *10*, 1001−1004.

(3) Fang, Z.; Liu, Z.; Wang, Y.; Ajayan, P. M.; Nordlander, P.; Halas, N. J. Graphene-antenna sandwich photodetector. *Nano Lett.* **2012**, *12*, 3808−3813.

(4) Cui, S.; Mao, S.; Lu, G.; Chen, J. Graphene coupled with nanocrystals: opportunities and challenges for energy and sensing applications. *J. Phys. Chem. Lett.* **2013**, *4*, 2441−2454.
(5) Konstantatos, G.; Badioli, M.; Gaudreau, L.; Osmond, J.; Bernechea, M.; De Arquer, F. P. G.; Gatti, F.; Koppens, F. H. Hybrid graphene−quantum dot phototransistors with ultrahigh gain. *Nat. Nanotechnol.* **2012**, *7*, 363−368.
(6) Fang, Z.; Thongrattanasiri, S.; Schlather, A.; Liu, Z.; Ma, L.; Wang, Y.; Ajayan, P. M.; Nordlander, P.; Halas, N. J.; García de Abajo, F. J. Gated tunability and hybridization of localized plasmons in nanostructured graphene. *ACS Nano* **2013**, *7*, 2388−2395.
(7) Bonaccorso, F.; Sun, Z.; Hasan, T.; Ferrari, A. Graphene photonics and optoelectronics. *Nat. Photonics* **2010**, *4*, 611.
(8) Koppens, F. H.; Chang, D. E.; Garcia de Abajo, F. J. Graphene plasmonics: a platform for strong light−matter interactions. *Nano Lett.* **2011**, *11*, 3370−3377.
(9) Reimann, S. M.; Manninen, M. Electronic structure of quantum dots. *Rev. Mod. Phys.* **2002**, *74*, 1283.
(10) Troparevsky, M. C.; Kronik, L.; Chelikowsky, J. R. Optical properties of CdSe quantum dots. *J. Chem. Phys.* **2003**, *119*, 2284−2287.
(11) Bhattacharya, P.; Ghosh, S.; Stiff-Roberts, A. Quantum dot opto-electronic devices. *Annu. Rev. Mater. Res.* **2004**, *34*, 1−40.
(12) Towe, E.; Pan, D. Semiconductor quantum-dot nanostructures: Their application in a new class of infrared photodetectors. *IEEE J. Sel. Top. Quantum Electron.* **2000**, *6*, 408−421.
(13) Kagan, C. R.; Murray, C. B. Charge transport in strongly coupled quantum dot solids. *Nat. Nanotechnol.* **2015**, *10*, 1013.
(14) Urban, J. J. Prospects for thermoelectricity in quantum dot hybrid arrays. *Nat. Nanotechnol.* **2015**, *10*, 997−1001.
(15) An, X.; Liu, F.; Jung, Y. J.; Kar, S. Tunable graphene−silicon heterojunctions for ultrasensitive photodetection. *Nano Lett.* **2013**, *13*, 909−916.
(16) Tang, J.; Kemp, K. W.; Hoogland, S.; Jeong, K. S.; Liu, H.; Levina, L.; Furukawa, M.; Wang, X.; Debnath, R.; Cha, D.; et al. Colloidal-quantum-dot photovoltaics using atomic-ligand passivation. *Nat. Mater.* **2011**, *10*, 765−771.
(17) Kramer, I. J.; Sargent, E. H. Colloidal quantum dot photovoltaics: a path forward. *ACS Nano* **2011**, *5*, 8506−8514.
(18) Tielrooij, K. J.; Orona, L.; Ferrier, A.; Badioli, M.; Navickaite, G.; Coop, S.; Nanot, S.; Kalinic, B.; Cesca, T.; Gaudreau, L.; et al. Electrical control of optical emitter relaxation pathways enabled by graphene. *Nat. Phys.* **2015**, *11*, 281−287.
(19) Lee, J.; Bao, W.; Ju, L.; Schuck, P. J.; Wang, F.; Weber-Bargioni, A. Switching individual quantum dot emission through electrically controlling resonant energy transfer to graphene. *Nano Lett.* **2014**, *14*, 7115−7119.
(20) Salihoglu, O.; Kakenov, N.; Balci, O.; Balci, S.; Kocabas, C. Graphene as a reversible and spectrally selective fluorescence quencher. *Sci. Rep.* **2016**, *6*, 33911.
(21) Salihoglu, O.; Kakenov, N.; Balci, O.; Balci, S.; Kocabas, C. Graphene-quantum dot hybrid optoelectronics at visible wavelengths. *ACS Photonics* **2018**, *5*, 2384−2390.
(22) Kagan, C.; Murray, C.; Nirmal, M.; Bawendi, M. Electronic energy transfer in CdSe quantum dot solids. *Phys. Rev. Lett.* **1996**, *76*, 1517.
(23) Zhitomirsky, D.; Voznyy, O.; Hoogland, S.; Sargent, E. H. Measuring charge carrier diffusion in coupled colloidal quantum dot solids. *ACS Nano* **2013**, *7*, 5282−5290.
(24) Vanmaekelbergh, D.; Liljeroth, P. Electron-conducting quantum dot solids: novel materials based on colloidal semiconductor nanocrystals. *Chem. Soc. Rev.* **2005**, *34*, 299−312.
(25) Kholmicheva, N.; Moroz, P.; Eckard, H.; Jensen, G.; Zamkov, M. Energy transfer in quantum dot solids. *ACS Energy Letters* **2017**, *2*, 154−160.
(26) Achermann, M.; Petruska, M. A.; Crooker, S. A.; Klimov, V. I. Picosecond energy transfer in quantum dot Langmuir- Blodgett nanoassemblies. *J. Phys. Chem. B* **2003**, *107*, 13782−13787.
(27) Praveena, M.; Mukherjee, A.; Venkatapathi, M.; Basu, J. Plasmon-mediated emergence of collective emission and enhanced quantum efficiency in quantum dot films. *Phys. Rev. B: Condens. Matter Mater. Phys.* **2015**, *92*, 235403.
(28) Haridas, M.; Basu, J.; Gosztola, D.; Wiederrecht, G. Photoluminescence spectroscopy and lifetime measurements from self-assembled semiconductor-metal nanoparticle hybrid arrays. *Appl. Phys. Lett.* **2010**, *97*, 083307.
(29) Haridas, M.; Basu, J.; Tiwari, A.; Venkatapathi, M. Photoluminescence decay rate engineering of CdSe quantum dots in ensemble arrays embedded with gold nano-antennae. *J. Appl. Phys.* **2013**, *114*, 064305.
(30) Tripathi, L.; Praveena, M.; Basu, J. Plasmonic tuning of photoluminescence from semiconducting quantum dot assemblies. *Plasmonics* **2013**, *8*, 657−664.
(31) Praveena, M.; Dutta, R.; Basu, J. Resonant Enhancement of Photoluminescence Intensity and Anisotropy of Quantum Dot Monolayers with Self-Assembled Gold Nanorods. *Plasmonics* **2017**, *12*, 1911−1919.
(32) Dutta, R.; Jain, K.; Venkatapathi, M.; Basu, J. Large emission enhancement and emergence of strong coupling with plasmons in nanoassemblies: Role of quantum interactions and finite emitter size. *Phys. Rev. B: Condens. Matter Mater. Phys.* **2019**, *100*, 155413.
(33) Anger, P.; Bharadwaj, P.; Novotny, L. Enhancement and quenching of single-molecule fluorescence. *Phys. Rev. Lett.* **2006**, *96*, 113002.
(34) Govorov, A. O.; Bryant, G. W.; Zhang, W.; Skeini, T.; Lee, J.; Kotov, N. A.; Slocik, J. M.; Naik, R. R. Exciton- plasmon interaction and hybrid excitons in semiconductor- metal nanoparticle assemblies. *Nano Lett.* **2006**, *6*, 984−994.
(35) Raja, A.; Montoya-Castillo, A.; Zultak, J.; Zhang, X.-X.; Ye, Z.; Roquelet, C.; Chenet, D. A.; van der Zande, A. M.; Huang, P.; Jockusch, S.; et al. Energy transfer from quantum dots to graphene and MoS2: The role of absorption and screening in two-dimensional materials. *Nano Lett.* **2016**, *16*, 2328−2333.
(36) Bawendi, M. G.; Steigerwald, M. L.; Brus, L. E. The quantum mechanics of larger semiconductor clusters (" quantum dots"). *Annu. Rev. Phys. Chem.* **1990**, *41*, 477−496.
(37) El-Sayed, M. A. Small is different: shape-, size-, and composition-dependent properties of some colloidal semiconductor nanocrystals. *Acc. Chem. Res.* **2004**, *37*, 326−333.
(38) Yin, Y.; Alivisatos, A. P. Colloidal nanocrystal synthesis and the organic−inorganic interface. *Nature* **2005**, *437*, 664−670.
(39) Castro Neto, A.; Guinea, F.; Peres, N. M.; Novoselov, K. S.; Geim, A. K. The electronic properties of graphene. *Rev. Mod. Phys.* **2009**, *81*, 109.
(40) Li, Z.; Qian, H.; Wu, J.; Gu, B.-L.; Duan, W. Role of symmetry in the transport properties of graphene nanoribbons under bias. *Phys. Rev. Lett.* **2008**, *100*, 206802.
(41) Yu, Y.-J.; Zhao, Y.; Ryu, S.; Brus, L. E.; Kim, K. S.; Kim, P. Tuning the graphene work function by electric field effect. *Nano Lett.* **2009**, *9*, 3430−3434.
(42) Chakraborty, B.; Gu, J.; Sun, Z.; Khatoniar, M.; Bushati, R.; Boehmke, A. L.; Koots, R.; Menon, V. M. Control of strong light−matter interaction in monolayer WS2 through electric field gating. *Nano Lett.* **2018**, *18*, 6455−6460.
(43) Kim, D.; Okahara, S.; Nakayama, M.; Shim, Y. Experimental verification of Förster energy transfer between semiconductor quantum dots. *Phys. Rev. B: Condens. Matter Mater. Phys.* **2008**, *78*, 153301.
(44) Wu, J.; Lu, Y.; Feng, S.; Wu, Z.; Lin, S.; Hao, Z.; Yao, T.; Li, X.; Zhu, H.; Lin, S. The Interaction between Quantum Dots and Graphene: The Applications in Graphene-Based Solar Cells and Photodetectors. *Adv. Funct. Mater.* **2018**, *28*, 1804712.
(45) He, W.; Qin, C.; Qiao, Z.; Gong, Y.; Zhang, X.; Zhang, G.; Chen, R.; Gao, Y.; Xiao, L.; Jia, S. In situ manipulation of fluorescence resonance energy transfer between quantum dots and monolayer graphene oxide by laser irradiation. *Nanoscale* **2019**, *11*, 1236−1244.

https://doi.org/10.1021/acs.jpcc.1c00643
J. Phys. Chem. C 2021, 125, 8314−8322

(46) Jeong, K. S.; Tang, J.; Liu, H.; Kim, J.; Schaefer, A. W.; Kemp, K.; Levina, L.; Wang, X.; Hoogland, S.; Debnath, R.; et al. Enhanced mobility-lifetime products in PbS colloidal quantum dot photovoltaics. *ACS Nano* **2012**, *6*, 89−99.
(47) Ip, A. H.; Thon, S. M.; Hoogland, S.; Voznyy, O.; Zhitomirsky, D.; Debnath, R.; Levina, L.; Rollny, L. R.; Carey, G. H.; Fischer, A.; et al. Hybrid passivated colloidal quantum dot solids. *Nat. Nanotechnol.* **2012**, *7*, 577−582.
(48) Goldberg, D.; Menon, V. M. Enhanced amplified spontaneous emission from colloidal quantum dots in all-dielectric monolithic microcavities. *Appl. Phys. Lett.* **2013**, *102*, 081119.
(49) Praveena, M.; Phanindra Sai, T.; Dutta, R.; Ghosh, A.; Basu, J. Electrically Tunable Enhanced Photoluminescence of Semiconductor Quantum Dots on Graphene. *ACS Photonics* **2017**, *4*, 1967−1973.
(50) Malard, L.; Pimenta, M. A.; Dresselhaus, G.; Dresselhaus, M. Raman spectroscopy in graphene. *Phys. Rep.* **2009**, *473*, 51−87.
(51) Beams, R.; Cançado, L. G.; Novotny, L. Raman characterization of defects and dopants in graphene. *J. Phys.: Condens. Matter* **2015**, *27*, 083002.
(52) Kovalenko, M. V.; Scheele, M.; Talapin, D. V. Colloidal nanocrystals with molecular metal chalcogenide surface ligands. *Science* **2009**, *324*, 1417−1420.
(53) Boles, M. A.; Ling, D.; Hyeon, T.; Talapin, D. V. The surface science of nanocrystals. *Nat. Mater.* **2016**, *15*, 141−153.
(54) Dong, A.; Ye, X.; Chen, J.; Kang, Y.; Gordon, T.; Kikkawa, J. M.; Murray, C. B. A generalized ligand-exchange strategy enabling sequential surface functionalization of colloidal nanocrystals. *J. Am. Chem. Soc.* **2011**, *133*, 998−1006.
(55) Nag, A.; Kovalenko, M. V.; Lee, J.-S.; Liu, W.; Spokoyny, B.; Talapin, D. V. Metal-free inorganic ligands for colloidal nanocrystals: S2−, HS−, Se2−, HSe−, Te2−, HTe−, TeS32−, OH−, and NH2−as surface ligands. *J. Am. Chem. Soc.* **2011**, *133*, 10612−10620.
(56) Nag, A.; Zhang, H.; Janke, E.; Talapin, D. V. Inorganic surface ligands for colloidal nanomaterials. *Z. Phys. Chem.* **2015**, *229*, 85−107.
(57) Liu, I.-S.; Lo, H.-H.; Chien, C.-T.; Lin, Y.-Y.; Chen, C.-W.; Chen, Y.-F.; Su, W.-F.; Liou, S.-C. Enhancing photoluminescence quenching and photoelectric properties of CdSe quantum dots with hole accepting ligands. *J. Mater. Chem.* **2008**, *18*, 675−682.
(58) Leatherdale, C.; Kagan, C.; Morgan, N.; Empedocles, S.; Kastner, M.; Bawendi, M. Photoconductivity in CdSe quantum dot solids. *Phys. Rev. B: Condens. Matter Mater. Phys.* **2000**, *62*, 2669.
(59) Yun, H. J.; Paik, T.; Edley, M. E.; Baxter, J. B.; Murray, C. B. Enhanced charge transfer kinetics of CdSe quantum dot-sensitized solar cell by inorganic ligand exchange treatments. *ACS Appl. Mater. Interfaces* **2014**, *6*, 3721−3728.
(60) Gómez-Santos, G.; Stauber, T. Fluorescence quenching in graphene: A fundamental ruler and evidence for transverse plasmons. *Phys. Rev. B: Condens. Matter Mater. Phys.* **2011**, *84*, 165438.
(61) Swathi, R.; Sebastian, K. Long range resonance energy transfer from a dye molecule to graphene has (distance)- 4 dependence. *J. Chem. Phys.* **2009**, *130*, 086101.
(62) Tisler, J.; Oeckinghaus, T.; Stohr, R. J.; Kolesov, R.; Reuter, R.; Reinhard, F.; Wrachtrup, J. Single defect center scanning near-field optical microscopy on graphene. *Nano Lett.* **2013**, *13*, 3152−3156.
(63) Gaudreau, L.; Tielrooij, K.; Prawiroatmodjo, G.; Osmond, J.; de Abajo, F. G.; Koppens, F. Universal distance-scaling of nonradiative energy transfer to graphene. *Nano Lett.* **2013**, *13*, 2030−2035.
(64) Hosoki, K.; Tayagaki, T.; Yamamoto, S.; Matsuda, K.; Kanemitsu, Y. Direct and stepwise energy transfer from excitons to plasmons in close-packed metal and semiconductor nanoparticle monolayer films. *Phys. Rev. Lett.* **2008**, *100*, 207404.
(65) Li, M.; Chen, J.-S.; Routh, P. K.; Zahl, P.; Nam, C.-Y.; Cotlet, M. Distinct Optoelectronic Signatures for Charge Transfer and Energy Transfer in Quantum Dot−MoS2 Hybrid Photodetectors Revealed by Photocurrent Imaging Microscopy. *Adv. Funct. Mater.* **2018**, *28*, 1707558.
(66) Chen, J.-S.; Li, M.; Wu, Q.; Fron, E.; Tong, X.; Cotlet, M. Layer-Dependent Photoinduced Electron Transfer in 0D−2D Lead Sulfide/Cadmium Sulfide-Layered Molybdenum Disulfide Hybrids. *ACS Nano* **2019**, *13*, 8461−8468.
(67) Marcus, R. A.; Sutin, N. Electron transfers in chemistry and biology. *Biochim. Biophys. Acta, Rev. Bioenerg.* **1985**, *811*, 265−322.
(68) Oevering, H.; Paddon-Row, M. N.; Heppener, M.; Oliver, A. M.; Cotsaris, E.; Verhoeven, J. W.; Hush, N. S. Long-range photoinduced through-bond electron transfer and radiative recombination via rigid nonconjugated bridges: distance and solvent dependence. *J. Am. Chem. Soc.* **1987**, *109*, 3258−3269.
(69) Williams, R. M. Distance and orientation dependence of photoinduced electron transfer through twisted, bent and helical bridges: a Karplus relation for charge transfer interaction. *Photochemical & Photobiological Sciences* **2010**, *9*, 1018−1026.

https://doi.org/10.1021/acs.jpcc.1c00643
J. Phys. Chem. C 2021, 125, 8314−8322